Applied Catalysis B: Environmental 187 (2016) 59–66

Contents lists available at ScienceDirect

Applied Catalysis B: Environmental

journal homepage: www.elsevier.com/locate/apcatb

Effects of electronic structure and interfacial interaction between metal-quinoline complexes and TiO_2 on visible light photocatalytic activity of TiO_2

Yanwei Huang[a], Qingkun Shang[a,*], Dan Wang[a], Shuang Yang[a], Hongyu Guan[a], Qin Lu[b,c], Shik Chi Tsang[b,**]

[a] Faculty of Chemistry, Northeast Normal University, Changchun 130024, China
[b] Department of Chemistry, University of Oxford, Oxford OX1 3QR, UK
[c] Naval Research Laboratory, Chemistry Division, Washington D.C. 20375-5342, USA

ARTICLE INFO

Article history:
Received 16 September 2015
Received in revised form 8 January 2016
Accepted 11 January 2016
Available online 14 January 2016

Keywords:
Interfacial interaction
Metal-quinoline complex
TiO_2
Visible light photocatalytic activity

ABSTRACT

Two metal-quinoline complexes, Fe(III)-8-hydroxyquinoline-5-sulfonic acid (Fe-HQS) and Er(III)-8-hydroxyquinoline-5-sulfonic acid (Er-HQS), were used as sensitizers of TiO_2 for improving visible light photocatalytic activity of TiO_2. UV–vis spectra, X-ray Diffraction, X-ray Photoelectron Spectroscopy, Scanning Electron Microscope and Transmission Electron Microscope were put to use to characterize the structure and morphology of Fe-HQS-TiO_2 and Er-HQS-TiO_2. The effects of interfacial electron transfer and energy level matching between each complex and TiO_2 were researched intensively. Er-HQS-TiO_2 and Fe-HQS-TiO_2 exhibited enhanced photocatalytic activity on photodecomposition of phenol in aqueous solution under visible light irradiation comparing to that of pure TiO_2. According to photoelectrochemical response property and theoretical calculation of energy levels, two possible energy matching modes and photoelectron transmission pathways were proposed to explain the effects of Fe-HQS and Er-HQS on the interfacial interaction between metal-HQS complex and TiO_2, and their different photocatalytic activities under visible light irradiation. The work in this paper indicated that metal-HQS complex with appropriate electronic structure and HOMO-LUMO energy levels relative to the band gap of TiO_2 played a major role in improving TiO_2 photocatalytic activity.

1. Introduction

Titanium dioxide has been one of the most promising photocatalysts for photochemical production of hydrogen and wastewater treatment due to its chemical stability, wide availability, energy-saving and non-toxicity [1–4]. However, since it can only be excited by ultraviolet light due to its wide band gap, its practical applications have been limited when the solar energy is used as the source of renewable energy [5–9]. Several approaches to extend TiO_2 adsorption to visible light, involving mainly either bulk doping or surface modification, have been developed through the last decades. In general, the dye-sensitization of semiconductors characterized by high potential of the upper edge of valence band realized through surface modification encompasses an electron injection from the excited dye to the conduction band of TiO_2 [10,11]. Many sensitizers such as pure organic dyes [12–14], metal-complexes [15,16], and ruthenium bipyridly derivatives [17–20] have been frequently used to modify TiO_2 so as to efficiently utilize the solar light for photocatalysis. It has been recognized that the applications of pure organic dyes and ruthenium complexes are restricted by the poor charge transfer and low photochemical stability of the former, and the cost and toxicity of the latter. It is, therefore, highly desirable to develop novel metal complexes which absorb strongly in the visible region of the solar light with energy levels capable of injecting excited electrons into TiO_2's conduction bands. Low cost and non-toxicity are also important factors to be considered in the development of these novel metal complexes.

8-hydroxyquinoline and its derivatives had been known for their excellent properties to transfer electrons in organic electroluminescent device (OELD). Many metal/8-hydroxyquinoline complexes with wide range visible light absorption can be easily obtained but the studies about the effects of metal/8-

* Corresponding author.
** Corresponding author.
E-mail addresses: shangqk995@nenu.edu.cn (Q. Shang), edman.tsang@chem.ox.ac.uk (S.C. Tsang).

http://dx.doi.org/10.1016/j.apcatb.2016.01.025
0926-3373/

hydroxyquinoline complexes on the visible light photocatalytic activity of TiO_2 are scarce. Shuhai Chen et al. reported that Fe-quinoline complexes can transfer photoelectrons to the conduction band of TiO_2 and be regenerated by the electron injection from Rhodamine B. This Si-doped TiO_2 exhibited stronger absorption in the visible region and showed higher visible light photocatalytic activity for the degradation of Rhodamine B in an aqueous solution than Si-doped TiO_2 alone and commercial TiO_2 [21]. Su et al. studied the sensitization mechanism of tris (8-hydroquinline-5-carboxylic acid)/iron (III) on TiO_2 anatase (101) surface using density functional theory. They found that the complex possesses a very small HOMO (highest occupied molecular orbital)-LUMO (lowest unoccupied molecular orbital) energy gap which allows for easy electron excitation from the HOMO to the LUMO. The energy of the HOMO, LUMO and Fermi level of TiO_2 was increased once the complex was adsorbed on TiO_2. The enhancement of the open-circuit photovoltage in dye-sensitized TiO_2 solar cells was obtained [22].

In the present work, we report the experimental and theoretical investigation of the effects of electronic structure and interfacial interaction between metal/8-hydroxyquinoline complexes and TiO_2 on the visible light photocatalytic activity of TiO_2. We have found that the molecular structures and the electronic structures of the complexes determine their energy levels of HOMO and LUMO, and further affected the electron transfer from complexes to TiO_2, which mainly determined the photocatalytic activity of TiO_2. Two metal/8-hydroxyquinoline complexes, Fe (III)/8-hydroxyquinoline-5-sulfonic acid (Fe-HQS) and Er(III)/8-hydroxyquinoline-5-sulfonic acid (Er-HQS), were synthesized and each was combined with TiO_2 nanoparticles as the sensitizer. Both Fe-HQS and Er- HQS had a narrow band gap and a strong visible light absorption. They can transfer photoelectrons to the conduction band of TiO_2 under visible light irradiation. After linked with metal-quinoline complexes, TiO_2 nanoparticles showed higher photocatalytic activity and photochemical stability during the photodecomposition of phenol in an aqueous solution than using TiO_2 nanoparticles alone. Our experimental results, which were supported by the theoretical calculations, explained the different photocatalytic activities of Er-HQS-TiO_2 and Fe-HQS-TiO_2 using two possible interfacial interactions. The work reported here has provided important insight on designing novel high-performance photocatalysts which will significantly broaden the application of TiO_2 in the field of photocatalytic degradation of organic pollutants.

2. Experimental

2.1. Synthesis

TiO_2 nanoparticles were synthesized by hydrothermal methods. Tetrabutyl titanate (2.0 mL) was added dropwise to anhydrous ethanol (5.0 mL) to form a transparent solution under stirring. De-ionized water (3.0 mL) was then added. After continuing stirring 0.5 h the above solution was transferred to a 25 mL polytetrafluoroethylene (PTFE) equipped autoclave for a hydrothermal crystal growth process. The sample was heated at 120 °C for 2 h and then cooled to room temperature naturally. The precipitate obtained via centrifugal separation was washed with de-ionized water and anhydrous ethanol before drying in a vacuum oven at 80 °C for 24 h. This precursor was calcined at 450 °C for 4 h to form TiO_2 nanoparticles.

Er- HQS complex was prepared by reflux method using anhydrous ethanol as solvent. HQS (3 mmol) was dissolved in 50 mL anhydrous ethanol. This solution was refluxed at 80 °C for 0.5 h before 50 mL $Er(NO_3)_3$ (1 mmol) aqueous solution was added dropwise under vigorous stirring. The mixture was continually refluxed for 8 h. The green precipitate was collected by filtration and washed several times with anhydrous ethanol before drying at 100 °C for 24 h.

Fe-HQS complex was obtained by the similar method. HQS (3mmoL) was added into 50 mL anhydrous ethanol and the solution was refluxed at 80 °C for 0.5 h. Then 10 mL aqueous solution containing 1mmoL of Fe $(NO_3)_3$ was added dropwise to the above solution under constant stirring and the color of suspension changed to black immediately. The mixture was continually refluxed for 3 h. The black precipitate was collected by filtration and washed several times with anhydrous ethanol before drying at 100 °C for 24 h.

Metal-HQS complex-TiO_2 nanocomposites were prepared as follows. TiO_2 nanoparticles (0.1 g) were added into 10 mL of metal-HQS complex aqueous solution. This mixture was transferred to a 40 mL autoclave, and the autoclave was sealed and maintained at selected temperatures (from 70 °C to 140 °C) for 3 to 11 h. After the autoclave was cooled to room temperature naturally, the product was collected by centrifugation and washed three times with absolute ethanol, then dried at 100 °C. For the purpose of comparison, HQS equivalent to the molar mass of metal-HQS was used to synthesize metal-free HQS-TiO_2 nanoparticles under the same condition.

2.2. Characterizations

Ultraviolet absorption spectra (UV) of metal-HQS complexes and UV–vis Diffuse Reflectance Spectra (DRS) of metal-HQS complex-TiO_2 composites were obtained on VARIAN CARY 500 Scan UV–vis-NIR Spectrophotometer. XRD patterns were analyzed with a Kigaku.D/Max-ra using Cu Kα radiation. The size and morphology were characterized by XL30ESEM-FEG Scanning Electron Microscopic (SEM) and JEOL 100CXIITransmission Electron Microscopy (TEM). The XPS analysis was carried out by Thermo ESCALAB 250 X-ray Photoelectron Spectrometer.

2.3. Photocatalytic evaluation

In a typical photolysis experiment, 50 mg of metal-HQS complex-TiO_2 nanocomposites was dispersed in an aqueous solution (total volume = 50 mL) containing 10 mg L^{-1} phenol. In order to facilitate adsorption equilibrium on the surface of the photocatalyst, the dispersion was stirred for 30 min in the dark. A trichromatic lamp (80 W) was used as the visible light source for the photocatalytic reactions. The light beam passed through a 400 nm long pass filter before reaching the photocatalytic cell which was air cooled to maintain a constant temperature. The phenol concentration was analyzed via a colorimetric method in which 4-amino-antipyrine and $K_3[Fe(CN)_6]$ were used as the reagents. The color change was monitored at 510 nm using a UV–vis Spectrophotometer.

2.4. Theoretical calculations

The geometries of the metal-HQS complexes were optimized using density functional theory (DFT) B3LYP method [23]. Considering the relativistic effect of metal atoms, CEP-121G basis set was adopted for Fe and Er atoms, while 6–31g* basis set was employed for the nonmetal atoms. On the basis of the optimized geometries, the frontier molecular orbitals compositions and energy levels of the complexes were analyzed. All calculations were performed using Gaussian 09W program.

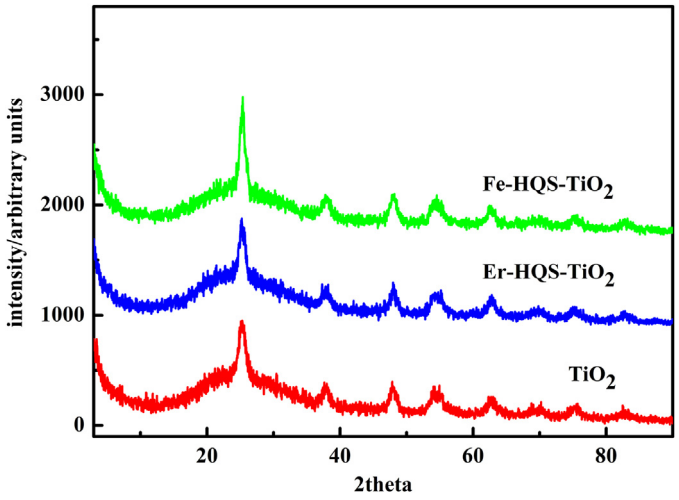

Fig. 1. XRD patterns of prepared TiO_2, Er-HQS-TiO_2 and Fe-HQS-TiO_2.

3. Results and discussion

3.1. Characterization of structure and morphology

The XRD patterns of TiO_2, Er-HQS-TiO_2 and Fe-HQS-TiO_2 are shown in Fig. 1. The characteristic peaks of anatase TiO_2 can be observed at 25.15°(101), 37.80°(004), 48.05°(200), 53.90°(105), 55.06°(211) and 62.69°(204) (JCPDS No.21-1272). There are no obvious diffraction peaks that could be attributed to other crystal structure of TiO_2. It can also be seen from Fig. 1 that the chief lattice plane for these three sample is {101} by comparing the intensities of diffraction peaks. The particle sizes of samples are calculated according to Debye-Scherrer formula and listed in Table 1. Both sizes of Er-HQS-TiO_2 (13.92 nm) and Fe-HQS-TiO_2 (13.67 nm) increased comparing to pure TiO_2 (12.24 nm). The crystal lattice parameters are also shown in Table 1. It is clear that the crystal lattice parameter a, b of Er-HQS-TiO_2 and Fe-HQS-TiO_2 only increased slightly relative to pure TiO_2. The obvious decrease of parameter c demonstrates a notable distortion of crystal structure of TiO_2 after forming nano-composities with Er-HQS and Fe-HQS.

Table 1
Particle sizes and crystal lattice parameters of samples.

samples	Crystal phase	Crystal size (nm)	Crystal parameter (nm)		
			a	b	c
TiO_2	Aantase	12.24	3.78676	3.78676	9.49135
Er-HQS-TiO_2-100 °C	Anatase	13.92	3.80639	3.80639	9.39336
Fe-HQS-TiO_2-100 °C	Anatase	13.67	3.80331	3.80331	9.40947

Fig. 2 shows the SEM and HRTEM images of pure TiO_2, Er-HQS-TiO_2 and Fe-HQS-TiO_2 nano-composites. All three samples are mainly composed of irregular spherical grains with average size about 13 nm, while many small particles aggregate to form large particles. Hydrogen bonds between hydroxyl groups on the surface of TiO_2 may cause this aggregation, while the interaction between sulfonic acid group of complex and hydroxyl group of TiO_2 may be another cause for aggregation.

The UV–vis absorption and diffuse reflectance spectra of M-HQS and M-HQS-TiO_2 were measured, as shown in Fig. 3. From Fig. 3a it can be found that the spectrum of HQS consists of two absorptions at 255 nm and 315 nm, corresponding to $\pi\rightarrow\pi^*$ and $n\rightarrow\pi^*$ transition of quinoline structure respectively. Another absorption peak at 360 nm is attributed to $n\rightarrow\pi^*$ transition from the substituent group $-SO_3H$. For Er-HQS and Fe-HQS complexes, the obvious blue shift of $\pi\rightarrow\pi^*$ absorption peaks can be found. It is noted that the $\pi\rightarrow\pi^*$ and $n\rightarrow\pi^*$electron transfer is restricted due to the formation of metal-quinoline conjugated structure. In addition, the absorptions at 400 nm (Er-HQS) and 432 nm (Fe-HQS) can be assigned to metal-ligand charge transfer (MLCT). For Fe-HQS, the absorption at 588 nm indicates the existence of d–d transition of Fe^{3+} under the disturbance of ligand field. Fig. 3b shows the diffuse reflectance spectra of TiO_2, Er-HQS-TiO_2 and Fe-HQS-TiO_2. The band gap of TiO_2 has been reduced from 3.2 eV to 2.68 eV (Er-HQS-TiO_2) and 2.63 eV (Fe-HQS-TiO_2), calculated using Kubelka-Munk formula $(Ahv)\,2 = (hv - Eg)$. That is to say, visible light response for

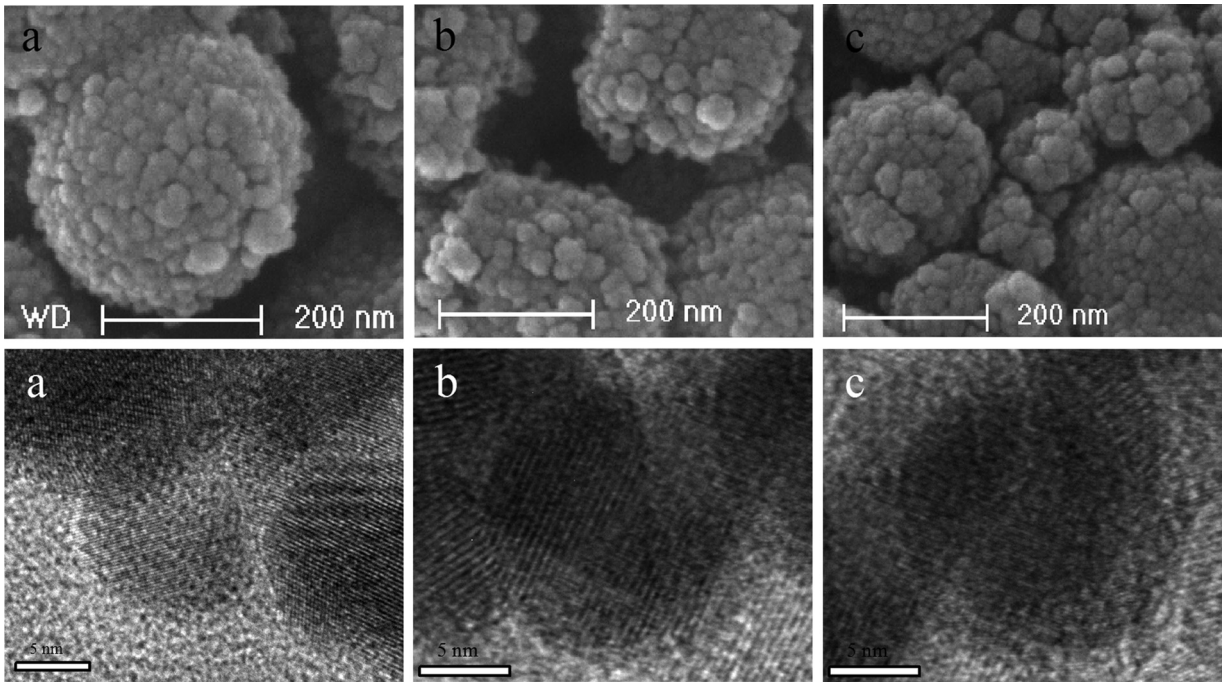

Fig. 2. SEM and HRTEM images of TiO_2 (a), Er-HQS-TiO_2(b) and Fe-HQS-TiO_2(c).

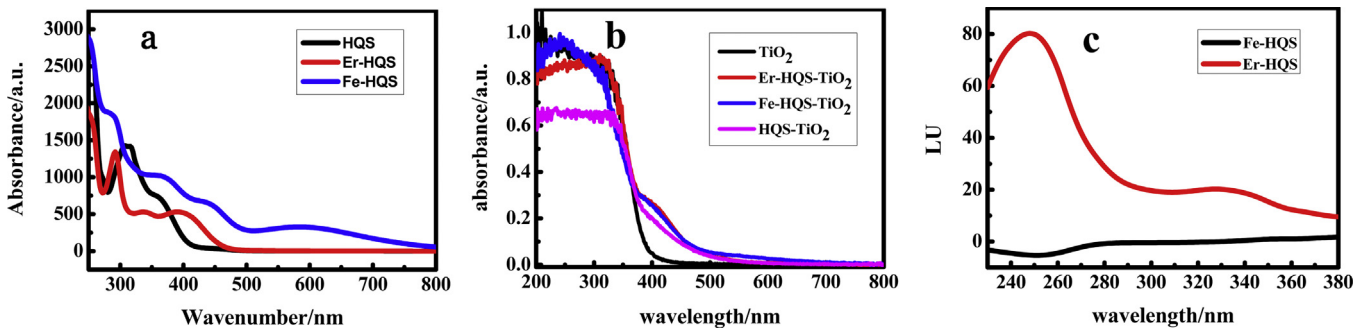

Fig. 3. Absorption spectra of M-HQS complexes (a), diffuse reflectance spectra of M-HQS-TiO_2(b) and upconversion emission spectra of M-HQS(c).

Er-HQS-TiO_2 and Fe-HQS-TiO_2 has obtained. Noticeably, Fe-HQS-TiO_2 shows stronger absorption in the range of 500–650 nm than Er-HQS-TiO_2. It is clear that the visible light absorption of Fe-HQS-TiO_2 and Er-HQS-TiO_2 are higher than that of HQS-TiO_2 prepared under the same condition.

Erbium is a typical rare earth element. In our previous work we studied its upconversion properties when it was doped in TiO_2 nanoparticles matrix. The green and red upconversion emission was observed under 980 nm laser excitation [24]. In Fig. 3c we have found that there are two upconversion emission peaks in UV region for Er-HQS upon the visible light excitation at 550 nm. Emission peak centered at 250 nm is attributed to the transition $^4D_{7/2}\rightarrow{}^4I_{15/2}$ of Er^{3+} and the peak at 330 nm to $^2P_{3/2}\rightarrow{}^4I_{15/2}$. It is worth mentioning that strong UV light emission from visible excitation of Er-HQS is especially useful for the visible light driven photocatalytic activity of Er-HQS-TiO_2 that will be discussed in the phenol photodegradation section. It is also clear from Fig. 3c that the upconversion emission is absent in Fe-HQS.

XPS experiments were carried out to collect further evidence that metal-HQS complexes formed nanocomposites with TiO_2. Figs. 4a,b shows the XPS high resolution spectra of Er-HQS-TiO_2 (4a) and Fe-HQS-TiO_2 (4b). Peaks at 458.8 eV, 464.6 eV in Fig. 4a and 458.85 eV, 464.55 eV in Fig. 4b belonging to Ti $2p_{3/2}$ and $2p_{1/2}$ indicate the existence of Ti^{4+} state. Relevant peaks' position are almost the same so caused the distances between peak $2p_{3/2}$ and $2p_{1/2}$ are 5.8 eV and 5.7 eV respectively, which demonstrates the crystal structure of TiO_2 does not change after combining with Fe-HQS or Er-HQS complex. At the same time peaks at 169 eV deriving from Er 4d and at 711 eV and 725 eV for Fe $2p_{1/2}$, Fe-$2p_{3/2}$ are detected. The appearance of peaks C 1s, O 1s, N 1s and S 2p illustrate the surface of TiO_2 has been contaminated by organic compounds. It is worth mentioning that peak O 1s attributed to Er-HQS-TiO_2 is different with that of Fe-HQS-TiO_2. For Er-HQS-TiO_2 peak at 532 eV belonging to hydroxyl oxygen (—OH) on the surface of TiO_2 is stronger that of other two peaks at 530 and 533.2 eV, that denotes lattice oxygen (Ti—O—Ti) in bulk phase of TiO_2, and C—O bond on the surface of TiO_2 respectively. But for Fe-HQS-TiO_2 not only the peak position(529.6, 530.05 and 531 eV) but also the intensity ratio of these three peaks change a lot comparing to that of Er-HQS-TiO_2. It is confirmed that the chemical surroundings of oxygen in these two nanomaterials are quite different.

3.2. Visible light photocatalytic activity and catalyst stability

To demonstrate the origin of phenol degradation upon visible light irradiation in the presence of Er-HQS-TiO_2, a series of parallel experiments were performed and the results are shown in Fig. 5a. First, phenol solution was irradiated for time t with visible light in the absence of catalyst. In this case, no degradation of phenol occurred. Second, a mixture of phenol solution and catalyst was kept for time t in the dark without irradiation. A very small amount of phenol was absorbed onto the nanocomposite's surface after time t, and the degradation ratio was negligible. And finally, phenol solution was irradiated for t time with visible light in the presence of TiO_2, HQS-TiO_2, and Er-HQS-TiO_2 respectively. It is found that 95.26% of phenol is decomposed in 3 h by Er-HQS-TiO_2 comparing to only 15.63% in the case of pure TiO_2. Results for photodegradation of phenol by using TiO_2, HQS-TiO_2, and Fe-HQS-TiO_2 are shown in Fig. 5b, and 94.49% of phenol is decomposed after 80 min in the presence of Fe-HQS-TiO_2. Both Er-HQS-TiO_2 and Fe-HQS-TiO_2 present significantly enhanced photocatalytic activity over pure TiO_2. It is worth to point out that the photcatalytic activity of HQS-TiO_2 is also higher than that of pure TiO_2 under the same condition, but weaker than that of Er-HQS-TiO_2 or Fe-HQS-TiO_2. The results suggest that the effective sensitization of TiO_2 from Er-HQS and Fe-HQS complexes, and HQS ligand alone, are realized. The sensitization is facilitated through the efficient electron injection from metal -HQS complex, or HQS, to the conduction band of TiO_2. In order to test the stability of the photocatalysts, the recycled photocatalytic experiments are carried out and the results are presented in Fig. 5c and d. The degradation efficiency of phenol decreases slightly after twice-recycled experiment for Er-HQS-TiO_2 and Fe-HQS-TiO_2, but the decrease is more noticeable for HQS-TiO_2.

The advantage of metal-HQS complex over HQS alone may be explained by the difference of their attachment modes to the surface of TiO_2. It has been demonstrated that the structure and the anchoring group of metal-HQS complexes or HQS on TiO_2 are crucial to the light harvesting and the charge injection at the metal-HQS complex/TiO_2 or HQS/TiO_2 interface, because they decide the amount of metal-HQS complex or HQS molecules attached to and their orientation on the surface of TiO_2 [25]. From Fig. 6, the schematic illustration of Er-HQS or HQS attached the surface of TiO_2, we can see that there are two possible modes linking HQS onto TiO_2 surface. One is chelating mode via N and O atoms of HQS coordinating to Ti atom of TiO_2 surface, and another is the binding of HQS sulfonate group with Ti of TiO_2 surface. These two modes compete with each other, causing the disorganization of HQS molecules on the surface of TiO_2, which may result in poor electron injection to the TiO_2 conduction band. The HQS molecules already attached to the surface of TiO_2 can also form hydrogen bonds with other HQS molecules using the remaining function groups. The aggregation increases the steric hindrance which can also reduce electron injection efficiency. Furthermore, hydrogen bonds formed between HQS can weaken the interaction between HQS and TiO_2 and decrease the stability of HQS-TiO_2 to some extent. On the contrary, the attachment of metal-HQS complex on the surface of TiO_2 via its anchoring sulfonate group provides a more compact and ordered arrangement which is obviously beneficial to the electron injection and the catalytic stability, which is confirmed by our experimental results.

Comparing Fig. 5a and b it is seen that shorter time (80 min) was needed to decompose the same amount of phenol using Fe-HQS-TiO_2 (3 h for Er-HQS-TiO_2). The different electronic structure and

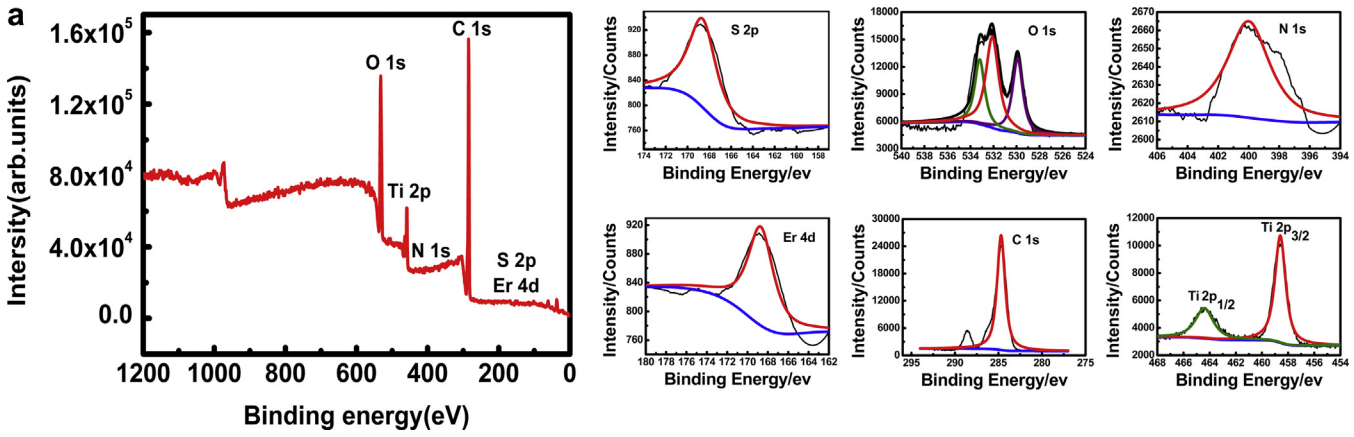

Fig. 4a. XPS spectra of Er-HQS-TiO_2.

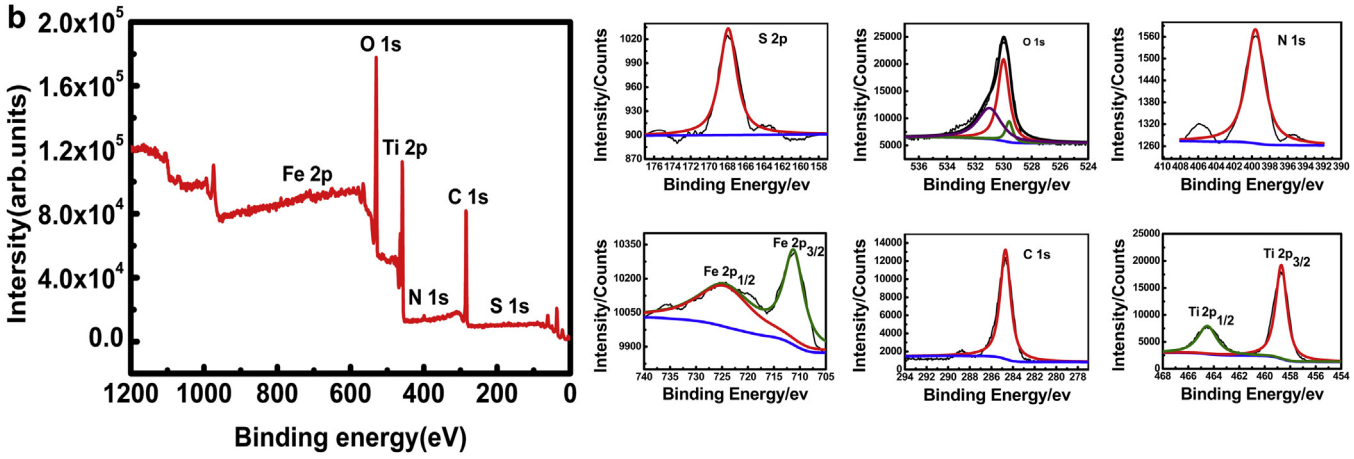

Fig. 4b. XPS spectra of Fe-HQS-TiO_2.

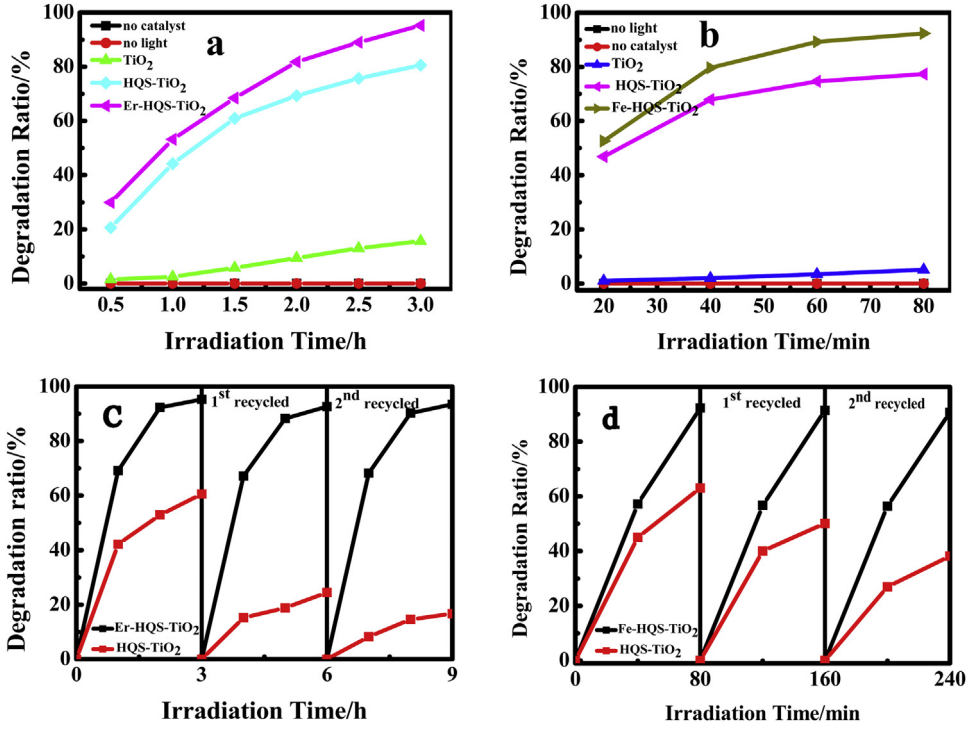

Fig. 5. Visible light degradation of phenol under different condition by Er-HQS-TiO_2 (a,c) and Fe-HQs-TiO_2 (b,d).

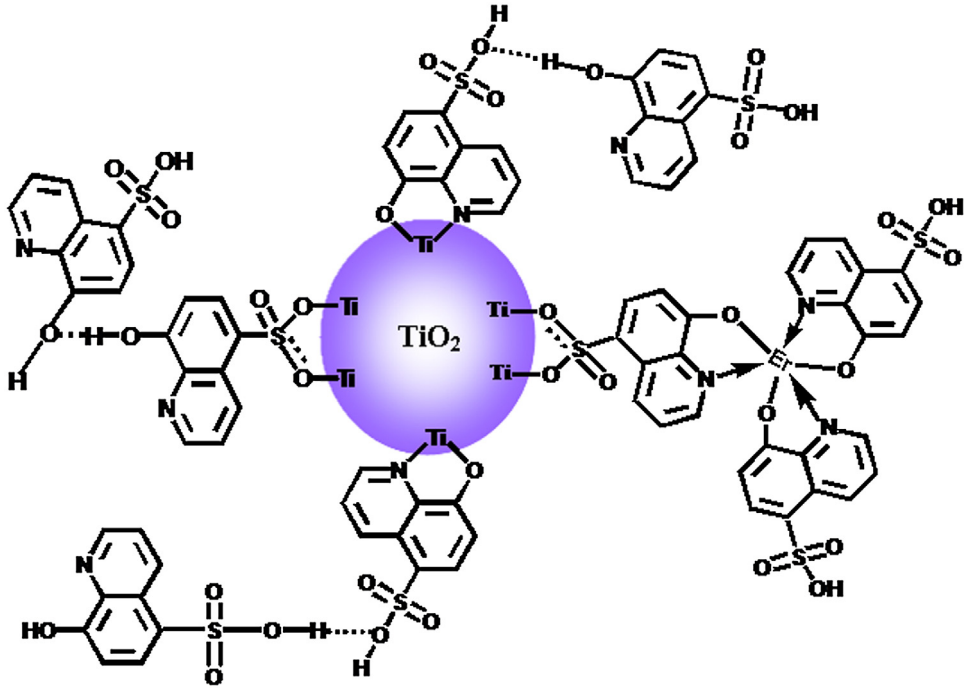

Fig. 6. Schematic illustration of M-HQS or HQS on the surface of TiO_2.

interfacial interaction between the metal complex and TiO_2 may be the key reason. On the one hand, the valence electron structures of transition metal Fe^{3+} and rare earth Er^{3+} are different. The valence electrons of Fe^{3+} are in the outermost 3d orbits, which is easy to transport excited electrons to ligand HQS via M-L transfer and then to the conduction band of TiO_2 when irradiated by visible light. However, the valence electrons of Er^{3+} are in 4f orbits, which are shielded effectively by outer 5s and 5p orbits. Instead of transferring excited electrons to the ligand and then to TiO_2, the f–f electron transitions take place inside the shell of 5s and 5p. This difference is revealed by their different energy requirement for M-L transfer: 432 nm for Fe-HQS, and 400 nm for Er-HQS.

To verify the effects of valence electron structure of metal ions on the interface electron transfer between metal-HQS complex and TiO_2, the photocurrent density of Fe-HQS-TiO_2 and Er-HQS-TiO_2 were recorded and given in Fig. 7. It is obvious that the photocurrent densities derived from TiO_2, Er-HQS-TiO_2 and Fe-HQS-TiO_2 are quite different when they are under visible light irradiation. As

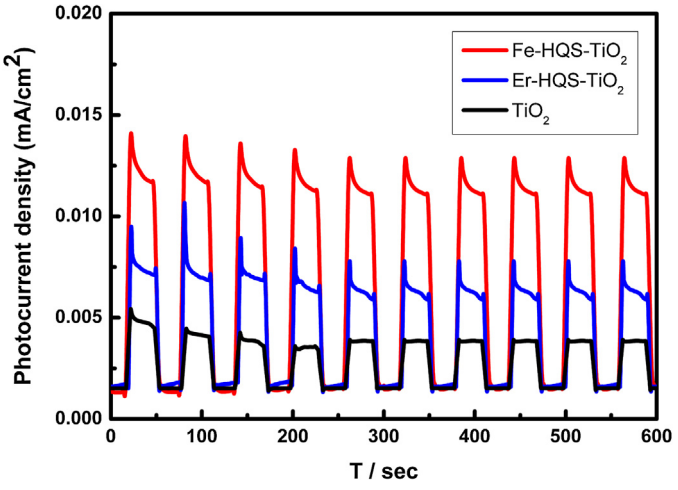

Fig. 7. Photoelectrochemistry performance of TiO_2, Er-HQS-TiO_2 and Fe-HQS-TiO_2.

soon as the visible light was turned on, the photocurrent densities for both Er-HQS-TiO_2 and Fe-HQS-TiO_2 reached their highest value, with faster response to visible light than TiO_2. During the process of irradiation the photocurrent densities of all three catalysts decreased slowly and changed slightly after ten circles, showing good photostability. The photocurrent densities of Fe-HQS-TiO_2 and Er-HQS-TiO_2 are, around three times and twice, respectively, higher than that of TiO_2. The higher the photocurrent density means the longer the lifetime of photo-generated charges, thus the better photocatalytic activity. It is no surprise that the best photoctatlytic activity is found for Fe-HQS-TiO_2.

On the other hand, interface electronic energy level alignment decides the efficiency of interfacial electron migration. Fig. 8 shows the diagrams of crucial molecular orbital energy levels of Fe-HQS and Er-HQS, The energy gap ΔE (LUM O-HOMO) relates with the visible light response of the metal-HQS complex, and the energy level matching or mismatching between the complex and TiO_2 determines the probability of electron transfer. From Fig. 8a it is found that the energy gap of Er-HQS (α isomer) is 1.716 eV and Er-HQS (β isomer) 3.371 eV, suggesting that the electron transfer from HOMO to LUMO can be achieved under visible light only for α isomer. It is clear that the electron cloud is concentrated around the central Er^{3+} ion after the electron excited from HOMO to LUMO. This situation is unfavorable for the enhancement of the photocatalytic activity of TiO_2, since it is the ligand rather than Er^{3+} ion that links to the surface of TiO_2. By contrast, the energy gap of Fe-HQS (α) and Fe-HQS (β) are 0.854 eV and 1.580 eV, respectively, meaning that visible light even near infrared light can be used to excite electrons from HOMO to LUMO. The benefit of electrons propagating from central Fe^{3+} to ligands (seen in Fig. 8b) is that photoelectrons are easy to inject to TiO_2 through ligand, which will improve the photocatalytic property of TiO_2.

Energy level matching between metal-HQS complex and TiO_2 is one of the most decisive factors for enhanced photocatalysis. Fig. 9 shows the schematic illustration of energy levels of Er-HQS, Fe-HQS and TiO_2. Between Er-HQS and TiO_2, photoelectrons are easy to move from LUMO of Er-HQS (α) to CB of TiO_2 under visible light irradiation due to energy level matching. Additionally, photoelectrons

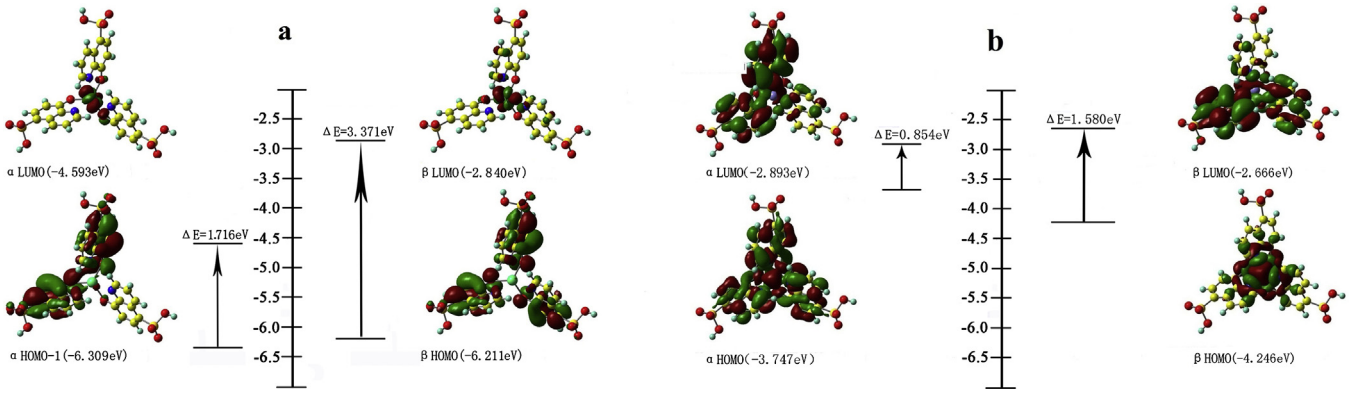

Fig. 8. Diagrams of crucial molecular orbital energy levels of Er-HQS (a) and Fe-HQS (b).

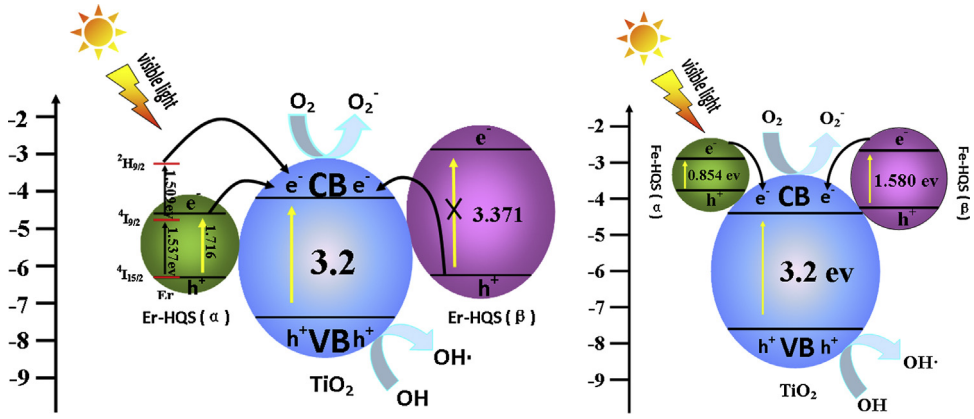

Fig. 9. Schematic illustration of energy level of Er-HQS, Fe-HQS and TiO_2.

on Er^{3+} energy level $^4I_{9/2}$ converging from ligands can be excited to $^2H_{9/2}$ first and then return to CB of TiO_2 via upconversion process. The injected electrons via either pathway are scavenged by the pre-adsorbed O_2 on the surface of TiO_2 to form superoxide anion radical, which with its strong oxidizing activity enables the degradation of phenol. These superoxide anion radicals attack the aromatic rings of organic pollutants forming intermediates and mineralizing them to carbon dioxide and water. A different situation exists for Fe-HQS-TiO_2. First, visible light is an effective excitation light source for both Fe-HQS (α) and Fe-HQS (β) because of their small energy gaps. Second, the CB energy of TiO_2 is lower than that of HOMO of both Fe-HQS (α) and Fe-HQS (β). So the photoelectrons on LUMO of Fe-HQS (α) and Fe-HQS (β) transfer to the CB of TiO_2 to decrease the whole energy of Fe-HQS-TiO_2 and increase the stability of system. The amount of photoelectrons obtained by TiO_2 is likely more than that in Er-HQS-TiO_2 since more effective photocatalysis in the decomposition of phenol is observed.

4. Conclusions

Er-HQS and Fe-HQS, with visible light adsorption, are stable, inexpensive, and easy to be synthesized. TiO_2 nanoparticles exhibited enhanced visible-light photocatalytic activity after sensitized with either of the two complexes. About 94.49% of phenol was decomposed after 80 min in the presence of Fe-HQS-TiO_2 under visible light irradiation (80W), while 3 h visible light irradiation was necessary to of the same amount of phenol when Er-HQS-TiO_2 was used as photocatalyst. The difference in photocatalytic activities of these two systems may be attributed to the different valence electronic structure and interfacial interactions between the complex and TiO_2, such as valence electron structures of metal ions, energy levels and electron transfer features of metal-HQS complexes, and the extent of energy level matching between metal-HQS complex and TiO_2. The work in this paper demonstrates that effective electron transfer at the interface of metal-HQS complex and TiO_2 together with the appropriate energy level alignment between the HOMO-LUMO of the metal complex and the band gap of TiO_2 is critical for metal-HQS-TiO_2 to achieve high visible light photocatalytic activity.

Acknowledgements

The authors would like to acknowledge the financial support by National Natural Science Foundation of China NSFC (21573039, 51102042), Jilin Province Science and Technology Development Project (20140414021GH, 200905932), Jilin Provence Environmental Protection Department Project (2008-22), and Jilin Province Personnel Department Project for supporting study abroad and return. We gratefully acknowledge Prof. Yongqing Qiu and Functional Materials Institute of Northeast Normal University for their helpful theoretical calculations.

References

[1] X. Chen, S.-S. Mao, Chem. Rev. 107 (2007) 2891–2959.
[2] J. Kim, J. Lee, W. Choi, Chem. Commun. 129 (2008) 756–758.
[3] J. Zeng, S. Liu, J. Cai, L. Zhang, J. Phys. Chem. C 114 (2010) 7806–7811.
[4] A. Fujishima, X.T. Zhang, D.A. Tryk, Surf. Sci. Rep. 63 (2008) 515–582.
[5] H. Tong, S.-X. Ouyang, Y.-P. Bi, N. Umezawa, M. Oshikiri, J.-H. Ye, Adv. Mater. 24 (2012) 229–251.
[6] R. Asahi, Y. Taga, W. Mannstadt, A. Freeman, Phys. Rev. B 61 (2000) 7459.
[7] A. Amtout, R. Leonelli, Phys. Rev. B 51 (1995) 6842.
[8] M. Koelsch, S. Cassaignon, C. Ta Thanh Minh, J.-F. Guillemoles, J.-P. Jolivet, Thin Solid Films 451 (2004) 86–92.

[9] W. Qin, D. Zhang, D. Zhao, L. Wang, K. Zheng, Chem. Commun. 46 (2010) 2304–2306.
[10] J.-H. Chen, C.-H. Tsai, S.-A. Wang, Y.-Y. Lin, T.-W. Huang, S.-F. Chiu, C.-C. Wu, K.-T. Wong, J. Org. Chem. 76 (2011) 8977–8985.
[11] J. Mei, K.R. Graham, R. Stalder, J.R. Reynolds, Org. Lett. 12 (2010) 660–663.
[12] M.-Q. Wang, X.G. Wang, Solar Energy Mater. Solar Cells 91 (2007) 1782–1787.
[13] B. Patrick, P. Kamat, J. Phys. Chem. 96 (1992) 1423–1428.
[14] Y. Park, S.-H. Lee, S.-O. Kang, W. Choi, Chem. Commun. 46 (2010) 2477–2479.
[15] W. Zhao, Y. Sun, F.N. Castellano, J. Am. Chem. Soc. 130 (2008) 12566–12567.
[16] W. Kim, T. Tachikawa, T. Majima, C. Li, H.-J. Kim, W. Choi, Energy Environ. Sci. 3 (2010) 1789–1795.
[17] E. Bae, W. Choi, J. Park, H.S. Shin, S.B. Kim, J.S. Lee, J. Phys. Chem. B 108 (2004) 14093–14101.
[18] Y. Cho, W. Choi, C.-H. Lee, T. Hyeon, H.-I. Lee, Environ. Sci. Technol. 35 (2001) 966–970.
[19] G. Li, K. Hu, C. Yi, K.L. Knappenberger Jr., G.J. Meyer, S.I. Gorelsky, M. Shatruk, J. Phys. Chem. C 117 (2013) 17399–17411.
[20] A.O.T. Patrocinio, K.P. Frin, N.Y. Murakami Iha, Inorg. Chem. 52 (2013) 5889–5896.
[21] R. Su, W.-D. Xue, Y. Feng, J.-H. Wang, D. Yi, Acta Phys. Chim. Sin. 25 (2009), 974–952.
[22] S.-H. Chen, B.-L. Lv, Y. Xu, Mater. Lett. 77 (2012) 32–34.
[23] M.J. Frisch, G.W. Trucks, H.B. Schlegel, G.E. Scuseria, M.A. Robb, J.R. Cheeseman, J.A. Montgomery Jr., T. Vreven, K.N. Kudin, J.C. Burant, J.M. Millam, S.S. Iyengar, J. Tomasi, V. Barone, B. Mennucci, M. Cossi, G. Scalmani, N. Rega, G.A. Petersson, H. Nakatsuji, M. Hada, M. Ehara, K. Toyota, R. Fukuda, J. Hasegawa, M. Ishida, T. Nakajima, Y. Honda, O. Kitao, H. Nakai, M. Klene, X. Li, J.E. Knox, H.P. Hratchian, J.B. Cross, V. Bakken, C. Adamo, J. Jaramillo, R. Gomperts, R.E. Stratmann, O. Yazyev, A.J. Austin, R. Cammi, C. Pomelli, J.W. Ochterski, P.Y. Ayala, K. Morokuma, G.A. Voth, P. Salvador, J.J. Dannenberg, V.G. Zakrzewski, S. Dapprich, A.D. Daniels, M.C. Strain, O. Farkas, D.K. Malick, A.D. Rabuck, K. Raghavachari, J.B. Foresman, J.V. Ortiz, Q. Cur, A.G. Baboul, S. Clifford, J. Cioslowski, B.B. Stefanov, G. Liu, A. Liashenko, P. Piskorz, I. Komaromi, R.L. Martin, D.J. Fox, T. Keith, M.A. Al-Laham, C.Y. Peng, A. Nanayakkara, M. Challacombe, P.M.W. Gill, B. Johnson, W. Chen, M.W. Wong, C. Gonzalez, J.A. Pople, Gaussian 09, Revision A.02, Gaussian Inc., Wallingford, CT, 2009.
[24] Q. Shang, H. Yu, X. Kong, H. Wang, X. Wang, Y. Sun, Y. Zhang, Q. Zeng, J. Lumin. 128 (2008) 1211–1216.
[25] V. Thavasi, V. Renugopalakrishnan, R. Jose, S. Ramakrishna, Mater. Sci. Eng. R 63 (2009) 81–99.